Nanoscale

PAPER

View Article Online
View Journal

Cite this: DOI: 10.1039/d5nr05082k

Insights into the role of common sulfur precursors in hydrothermally synthesized N,S-doped carbon dots: fluorescence modulation *via* surface oxidation rather than sulfur doping

Sónia Fernandes, [a] Manuel Algarra, *[b] Ana T. S. C. Brandão, [c] Antonio Gil,[b] Carlos M. Pereira, [c] Joaquim C. G. Esteves da Silva [a] and Luís Pinto da Silva *[a]

While heteroatom doping is widely used to enhance the fluorescence of carbon dots, the actual mechanism underlying this claimed enhancement remains unclear. Herein, we report a systematic comparison between nitrogen-doped carbon dots (N-CDs) and nitrogen/sulfur co-doped carbon dots (N,S-CDs) synthesized hydrothermally, with ethylenediamine and sodium thiosulfate as the N- and S-dopants, respectively. Contrary to expectations, the inclusion of the S-precursor significantly reduced the quantum yield by 63%, from 35.9% to 13.2%, while leaving the emission profile and response largely unchanged. Characterization assays revealed that S-doping in N,S-CDs was residual, whereas the surface oxygen content increased markedly, indicating surface oxidation. The data suggest that sodium thiosulfate acted not as a dopant but overall as an oxidant, generating oxygen-based surface defects that introduced nonradiative recombination pathways. Thus, our findings show that co-doping with this S-precursor can decrease the quantum yield by promoting surface oxidation and the effective formation of more oxidized N-CDs, rather than heteroatom incorporation and production of co-doped CDs. This decreasing effect on the quantum yield was also observed when using thiourea as the S-precursor. Future work should include the study of other common S-precursors. In conclusion, our research shows that specific heteroatom-based precursors can alter the optical characteristics of CDs through redox/surface-modification effects instead of actual compositional doping, and thus, claims based on heteroatom doping may need closer examination.

Received 2nd December 2025,
Accepted 20th March 2026

DOI: 10.1039/d5nr05082k

rsc.li/nanoscale

Introduction

Carbon dots (CDs) are a type of carbon-based nanomaterial, with sizes typically lower than 10 nm, and known for their fluorescence, biocompatibility, (photo)chemical stability, water solubility, and tunability.[1–3] These characteristics make CDs highly attractive for a range of applications, including in light-emitting devices, bioimaging, photocatalysis, and sensing.[4–6]

Another attractive feature of CDs is that they can potentially be generated from a variety of renewable carbon sources using environmentally friendly and non-toxic bottom-up routes.[7] This is particularly relevant when considering the development of engineered nanomaterials with a "sustainable-by-design" approach, given that the fabrication stage of nanomaterials has been identified as a potential environmental concern.[8–11] More specifically, CDs can be obtained from a wide variety of organic waste, such as agricultural (*e.g.*, corn stover and rice husks), food (*e.g.*, fruit peels and nut shells), urban waste (*e.g.*, spent coffee grounds), forestry residues (*e.g.*, eucalyptus leaves), and industrial byproducts (*e.g.*, sugarcane bagasse, olive pit liquor, and seafood shells).[5,12–15]

While CDs are known for their fluorescence and are used in fluorescence-based applications, their intrinsic quantum yield can be low (for both waste- and non-waste-based CDs).[16–20] Thus, CD synthesis processes typically involve heteroatom-doping strategies, in which compounds containing desired heteroatoms (such as N, S, P, and B) are added as dopants, resulting in the incorporation of these elements into the resulting nanoparticles.[21,22] The rationale behind this type of strategy is that heteroatom doping generates additional electron lone pairs, defect sites, and active centers, which facilitate radiative recombination and markedly enhance the fluorescence efficiency of CDs.[23–25]

[a]*Chemistry Research Unit (CIQUP), Institute of Molecular Sciences (IMS), Department of Geosciences, Environment and Spatial Plannings, Faculty of Sciences, University of Porto, R. Campo Alegre s/n, 4169-007 Porto, Portugal. E-mail: luis.silva@fc.up.pt*
[b]*INAMAT[2]-Institute for Advanced Materials and Mathematics, Department of Science, Public University of Navarra, Campus of Arrosadía, 31006 Pamplona, Spain*
[c]*Chemistry Research Unit (CIQUP), Institute of Molecular Sciences (IMS), Department of Chemistry and Biochemistry, Faculty of Sciences, University of Porto, R. Campo Alegre s/n, 4169-007 Porto, Portugal*

Among the various possible options, the most common doping strategies are arguably N-doping and N,S-doping, with S-doping being less employed.[21–24,26] Commonly used N-dopants are urea, ethylenediamine (EDA), and phenylenediamine, among others.[19,27–29] Regarding S-dopants, typical ones are $Na_2S_2O_3$, H_2SO_4, and Na_2S, among others.[21,22,30] Besides binary dopant systems (such as phenylenediamine/$Na_2S_2O_3$, urea/H_2SO_4, and EDA/H_2SO_4), single-source N,S-dopants (*e.g.*, cysteine and thiourea) can also be used.[31–34] Relevantly, both N- and N,S-doping strategies have been associated with high fluorescence quantum yields (QY_{FL}) and even red-shifted emission.[24,26,35–38]

However, despite these apparently promising reports of the potential of heteroatom-doping strategies for QY_{FL} enhancement, there are still unclarified issues that prevent their rational use in the fabrication of suitable and sustainable CDs for commercial/industrial applications.

For one, while different authors claim that N-doping is a suitable strategy for enhancing the QY_{FL} of CDs, there are different studies that either did not find any clear relationship between N-doping and the resulting QY_{FL} or concluded that N-doping alone is not enough for QY_{FL} enhancement.[4,39–41] Furthermore, studies that associate higher QY_{FL} with N-doping tend not to synthesize and study the corresponding non-N-doped CDs.[42,43] Without this comparison, it is ambiguous whether the observed high QY_{FL} values are related to the inclusion of nitrogen heteroatoms in the structure of CDs. Finally, it is known that bottom-up synthesis routes used to produce CDs can also generate highly fluorescent molecular by-products,[44–46] which can mask the luminescence of CDs. Furthermore, dialysis is considered an essential step to separate these by-products from CDs.[45,47,48] Despite this, several studies reporting N-CDs with elevated QY_{FL} did not incorporate adequate purification methods, and so, it is possible that the observed yields are not from CDs but from molecular fluorophores present in solution.[37,49,50]

Thus, the literature indicates that despite the widespread use of N-doping as a strategy for enhancing QY_{FL}, there are significant doubts about its overall success and potential, as well as its actual mechanism of action. Relevantly, while the N,S-doping strategy is relatively less used and studied than N-doping, there are some indications that the efficiency of the former as a general strategy should be equally questioned.

For one, there are also reports of highly emissive N,S-CDs (over 50%), but they did not include proper purification (as by dialysis).[51–54] This means that there is a question of whether the high QY_{FL} results from the N,S-CDs or from fluorescent molecular by-products. Some studies that also report highly emissive N,S-CDs did not include comparison with mono-doped and/or undoped CDs. Thus, it is also unclear whether the observed values result from synergistic effects of combining S- with N-doping.[52,55,56] Finally, there are also a number of synthesized N,S-CDs whose QY_{FL} values are still low ($\leq$~10%).[57–60] Therefore, there are discrepancies between the expected benefits of N,S-doping and the observed results.

Herein, we report the systematic characterization and comparison of N,S-CDs and N-CDs obtained from the hydrothermal treatment of sawdust and citric acid (as co-carbon precursors), EDA (as the N-dopant), and $Na_2S_2O_3$ (as the S-dopant). Our main goal is to gain insight into the role of combined N,S-doping regarding the optical properties and composition of CDs. The resulting data are essential to understand the true impact of N,S-doping as a QY_{FL}-enhancement strategy, with the systematic comparison with N-CDs allowing for the evaluation of whether combined doping results in any synergistic or additive effects. To this end, we performed comprehensive optical, microscopic, and structural characterization of both CDs, by using atomic force microscopy (AFM), X-ray photoelectron (XPS), Fourier-transform infrared (FTIR), X-ray diffraction (XRD), electron paramagnetic resonance (EPR), UV-Vis spectroscopy, steady-state fluorescence spectroscopy, and dynamic light scattering (DLS).

Notably, our results indicate that, contrary to potential expectations, combined N,S-doping reduces the QY_{FL} from 35.9% to 13.2% (a ~63% reduction) when compared with N-CDs. Despite these large alterations in QY_{FL}, the optical properties of both CDs (studied in different media and in the presence of different quenchers) were rather similar, which indicates that including $Na_2S_2O_3$ as a co-dopant had a limited effect. Finally, it was observed that the incorporation of S into the CDs was not effective and that $Na_2S_2O_3$ did not act as a true S-dopant (contrary to expectations). However, its use had an oxidative effect, resulting in surface oxidation of the CDs and a lower QY_{FL}. Thus, this study provided new insight into the efficiency of N,S-doping strategies for QY_{FL} enhancement, as well as some mechanistic insight into the role of dopant precursors in the synthesis of CDs and how they can modulate the nanomaterials' properties in unexpected ways.

Results and discussion

In this study, CDs were obtained through the hydrothermal treatment of the precursor mixture, which requires mild experimental conditions, is easy to operate, and is safe and low-cost.[12,61] It can be regarded as a representative method for creating these nanomaterials since it is also a common synthesis pathway for the creation of CDs.[13,15,20,23,57]

Citric acid was chosen as a co-carbon precursor, as it is arguably one of the most widely used traditional carbon sources for CD production.[25,27,37,41,62] Sawdust, a residue of the wood industry, was included as a co-carbon precursor, in a 50 : 50 mass ratio with citric acid. Its inclusion allowed for replacing half of the commercial carbon source with organic waste, which has already been shown to be an effective method for mitigating the environmental effects of CD manufacturing.[12,13] Both EDA and $Na_2S_2O_3$ are common N- and S-dopants,[26,34,40,63] respectively, and they were used as a binary doping system to generate N,S-CDs. For N-CDs, only EDA was used.

It is worth highlighting that we have selected widely used synthesis routes and common precursors to ensure that the conclusions obtained here are not limited to highly specific

conditions but instead provide insights that are broadly relevant to this field of research. The synthesis procedures here used are also based on a synthesis strategy developed previously by us for the generation of brightly fluorescent waste-based CDs.[12] The details of the synthesis procedures are provided in the Experimental section.

Optical characterization of CDs

The study began with a comparative characterization of the optical properties of N,S-CDs and N-CDs, toward understanding the resulting effect of S-inclusion on bi-doped CDs.

The fluorescence of both CDs was initially analyzed by measuring their 2D excitation–emission contour plots (EECPs), which are shown in Fig. 1. Interestingly, the two CDs exhibit a similar fluorescence profile, with the EECPs exhibiting a well-defined and single luminescent center, characterized by an emission maximum at ~440 nm and an excitation maximum at ~350 nm. This indicates that going from mono- to bi-doped CDs, with inclusion of S, had a limited effect on the properties of CDs. Moreover, and contrary to potential expectations, the inclusion of an S-dopant did not lead to a red-shifted emission.[24,26]

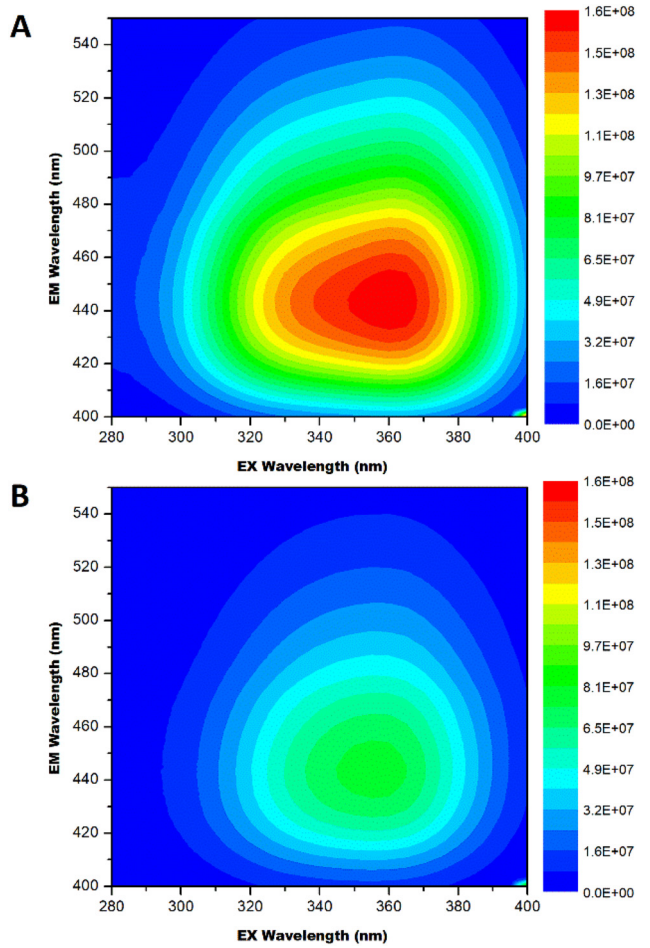

Fig. 1 EECPs of N-CDs (A) and N,S-CDs (B) in water.

The emission spectrum of each CD, measured at an excitation wavelength of 350 nm, is also presented (Fig. 2). The spectral shapes (Fig. 2A) are similar between CDs and are consistent with published spectra for this type of nanomaterial.[12] The emission spectrum of N-CDs is slightly broader than that of N,S-CDs (Fig. 2B), as can be seen from their full width at half maximum (FWHM) values of 79.4 and 73.5 nm, respectively. Nevertheless, this difference is rather modest. Interestingly, we can still see that the fluorescence intensity of N,S-CDs is lower than that of N-CDs, at the same concentration (Fig. 2A).

The UV-Vis spectra of the CDs were also recorded (Fig. 2C). The spectrum of N-CDs exhibited an absorption band with a maximum at 350 nm (attributed to n → π* transitions) and two small shoulders at ~240 nm and ~280 nm that were associated with π → π* transitions. Interestingly, the spectrum of N,S-CDs did show some relevant differences. Namely, while still present, the relative intensity of the 350 nm band is greatly reduced, and the shoulder at 240 nm is now not clearly visible. The shoulder at ~280 nm is still seen, nevertheless. Thus, the data indicate that the addition of an S-dopant affects the surface or structural features of these CDs.

The QY_{FL} values of the CDs were also determined by a relative method using quinine sulfate as a reference and were found to be 35.9% and 13.2% for N-CDs and N,S-CDs, respectively. It should be noted that the QY_{FL} obtained for N-CDs is relatively high, given that waste-based CDs tend to have a relatively low QY_{FL} (below 20%).[17–20] Thus, the followed synthesis strategy was useful for obtaining brightly emissive waste-based CDs.[12] Nevertheless, the co-addition of an S-dopant did not result in the predicted effect.[21,30–34,52,55,57,58] That is, in a QY_{FL} enhancement. In contrast, the use of an S-dopant decreased the QY_{FL} by 63%. Furthermore, even when considering just the QY_{FL} of N,S-CDs, a value of 13.2% is rather modest. Thus, for this system, adding an S-dopant in a binary system with an N-dopant not only does not produce brightly emissive CDs but also impairs fluorescence efficiency. This adds more doubts about the true benefits of heteroatom-doping strategies as a general solution for enhancing the QY_{FL} of CDs.

We also examined the relationship between the absorbance at 350 nm and the mass concentration of each CD (Fig. 2D). The variation was more significant for N-CDs than for N, S-CDs, which indicates that the former are stronger absorbers on a mass basis. Thus, not only does co-S-doping reduce the QY_{FL}, but it may also impair fluorescence intensity by reducing the light-absorption potential of the CDs.

In summary, so far, while co-S-doping has had little effect on the emission band position and shape, it has impaired the fluorescence efficiency of the CDs, while also affecting their surface/structural features. To gain further insight into the effects of this co-doping strategy on the optical properties of CDs, we performed additional fluorescence assays under various conditions.

In the initial assays, we aimed to investigate the fluorescence behavior of the CDs by measuring their emission intensity in water/methanol and water/glycerol mixtures with

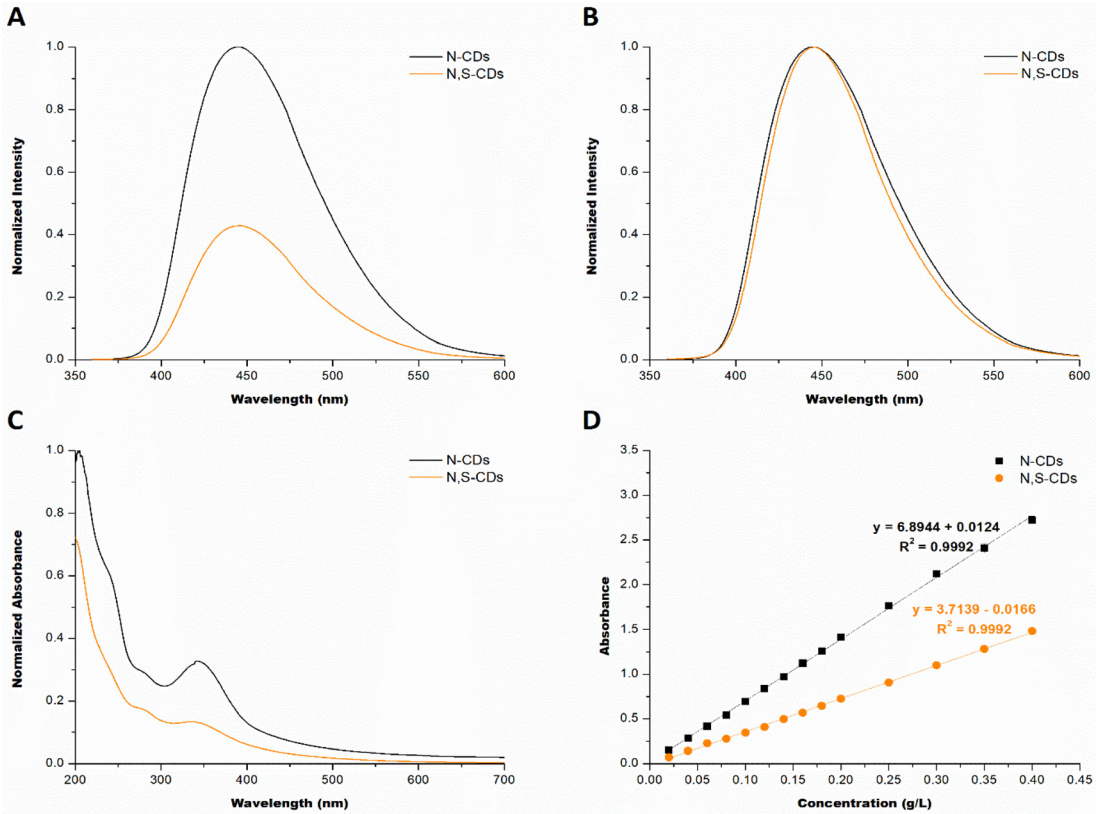

Fig. 2 Emission (A) and normalized emission (B) spectra of N-CDs and N,S-CDs; UV-Vis spectra of N-CDs and N,S-CDs (C); and absorbance as a function of concentration for both CDs (D).

increasing water content (Fig. 3). With these mixtures, we tried to probe the effect exerted by solvent polarity and viscosity (respectively). Interestingly, both CDs had the same behavior in these scenarios. That is, increasing the water percentage in both mixtures did not have a significant alteration in the fluorescence intensities of the nanoparticles, except just in both pure methanol and glycerol, but even then, the difference compared to pure water is somewhat modest. Therefore, these data indicate that the excited states of N-CDs are not strongly affected by solvent polarity and that nonradiative decay due to intramolecular motion does not appear to be relevant.[64–66] Additionally, co-S-doping did not alter these outcomes.

We subsequently evaluated the effects exerted by KI and KNO_3 on the fluorescence of N-CDs and N,S-CDs (Fig. 4). KI is a well-known heavy-atom quencher, given that its addition can result in fluorescence quenching by enhancing intersystem crossing in organic fluorophores.[62,67,68] KNO_3 was selected to evaluate the potential effect of another small ionic compound that shares the same counter-cation as KI but has different characteristics. Specifically, while KI can act as a hole scavenger, KNO_3 is known to function as an electron scavenger.[69,70]

Both ionic compounds induced quenching in the two CDs, and the resulting Stern–Volmer plots (Fig. 4) showed a linear relationship, which is usually associated with dynamic quenching. However, the quenching was rather limited in both cases, given that the obtained Stern–Volmer constants (K_{SV}) were only 5.1–6.7 × 10^{-3} and 3–5 × 10^{-4} mM^{-1}, in the presence of KI and KNO_3, respectively. Nevertheless, these assays did allow us to make two conclusions: (1) the CDs are more sensitive to KI than to KNO_3, probably due to the heavy-atom quenching effect of the former;[62,71] and (2) the fluorescence of N,S-CDs appears to be more sensitive to both quenchers than that of N-CDs (Fig. 4), which indicates some effect exerted by the co-S-doping.

In Fig. S1A, the relationship between fluorescence intensity and absorbance for N-CDs and N,S-CDs is presented. Both CDs showed the trend of a general increase in fluorescence intensity with increasing absorbance, which is not an unexpected behavior. Nevertheless, some studies have shown a decrease in fluorescence intensity with increasing concentration of CDs, which is attributed to aggregation-caused quenching (ACQ) and self-absorption quenching.[72,73] Thus, these results indicate that neither ACQ nor self-absorption quenching plays a relevant role within this absorbance range.

The photostability of the CDs was also tested by continuous irradiation at 365 nm for 30 minutes (Fig. S1B). Interestingly, both CDs were found to be photostable, with F/F_0 remaining constant throughout the assays. This stability suggests their suitability for optical applications, where sustained fluorescence is required under prolonged exposure to light.

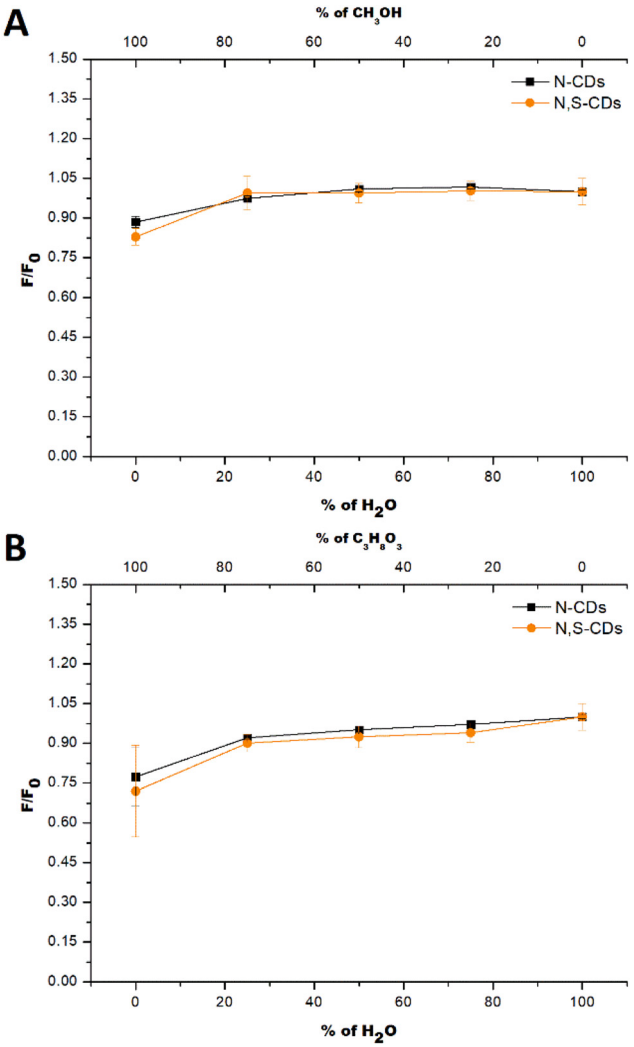

Fig. 3 Variation in fluorescence emission intensity in water/methanol (A) and water/glycerol (B) mixtures for N-CDs and N,S-CDs. Excitation at 350 nm.

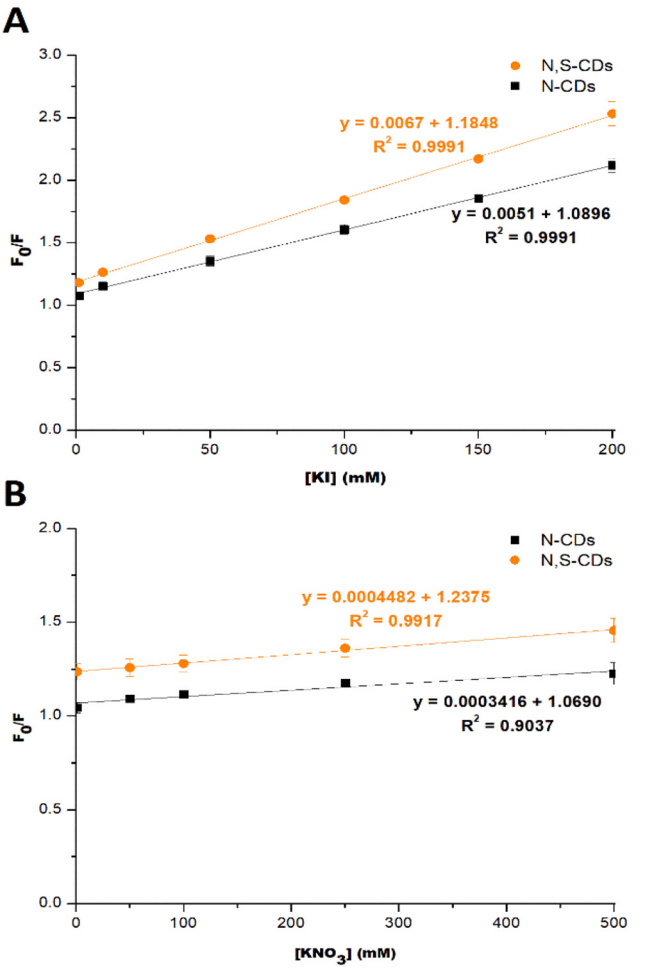

Fig. 4 Stern–Volmer plots for different quenchers: KI (A) and KNO_3 (B), for both CDs.

Furthermore, the behavior of both CDs was identical, meaning that co-S-doping had no effect on this characteristic.

The influence of the solvent on the fluorescence of the CDs was further probed through assays in water, methanol, ethanol, acetonitrile, and dimethylformamide (DMF), as presented in Fig. 5. Fig. 5A and C enable the measurement of the shift in the emission wavelength maximum caused by the solvent for N-CDs and N,S-CDs, respectively. Specifically, there is a little blue shift of about 10 nm from water to acetonitrile/DMF in both CDs. The variations in fluorescence intensity with solvent can be better observed in Fig. 5B (N-CDs) and Fig. 5D (N,S-CDs). Once again, the CDs behave similarly, with an ~20% (slightly higher for N,S-CDs) decrease in intensity from water to acetonitrile/DMF. These changes can be attributed to the different hydrogen-bonding interactions that the CDs can make with the solvent. That is, we observed variations associated with changing from protic to aprotic solvents, and there are reports in the literature that indicate that the fluorescence of CDs can be more significantly modulated by hydrogen bonding than by solvent polarity.[74]

Furthermore, the fluorescence emission behavior of both CDs was also analyzed in the same solvents using the Reichardt solvent polarity scale, ET(30). The results indicate that both N-CD and N,S-CD samples exhibit similar emission maxima (Fig. S2A) across different solvents, suggesting a limited solvatochromic effect. Fig. S2B shows comparable trends in fluorescence intensity ratios (F/F_{H_2O}). Additionally, the regression slopes observed in Fig. S2B indicate that both samples respond similarly to changes in solvent polarity, with only minor variations in fluorescence intensity.

One matter of debate regarding CDs is the origin of their fluorescence, and the relative relevance between core and surface states in their emission.[75–77] Here, we performed a comprehensive analysis of the fluorescence of the two CDs studied, specifically, by assessing their responses to external stimuli (ionic quenchers) and modifications in the external media (solvent polarity, hydrogen bonding, and viscosity). It is interesting to note that we have discovered that both CDs are virtually unaffected by these variations, exhibiting only slight

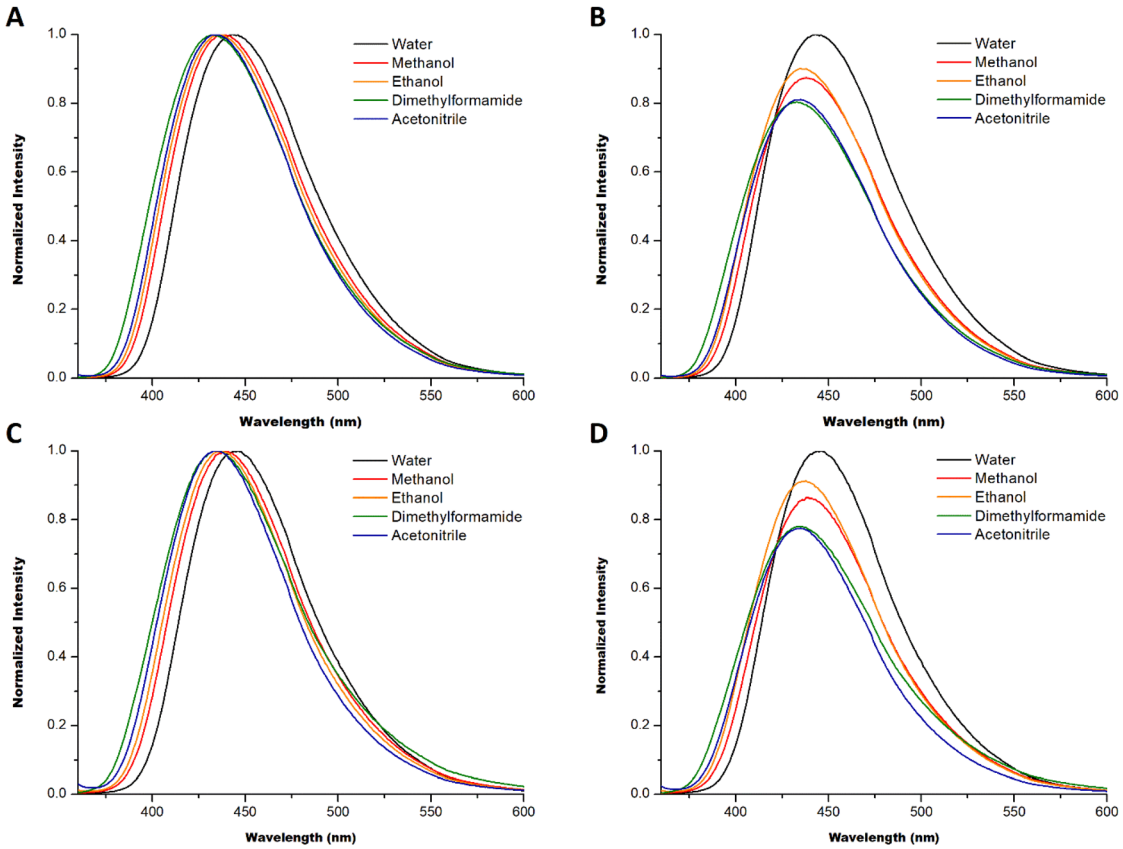

Fig. 5 Normalized emission spectra for evaluation of maximum emission wavelength and emission intensity of N-CDs (A and B, respectively) and N,S-CDs (C and D, respectively) in different solvents.

alterations. This suggests that their fluorescent moieties are partially protected from outside stimuli and media. This implies that their predominant emissive states are probably connected to core or protected states rather than less accessible surface-related ones.[4]

It should be noted that while N,S-CDs are, to a great extent, almost as unresponsive as N-CDs to these stimuli/changes, the resulting variations are slightly more relevant. Thus, it appears that the fluorescent moieties of N,S-CDs are somewhat less protected from the external environment, but co-S-doping does not change the overall situation.

Therefore, the emission of N,S-CDs appears to have a greater contribution from more surface-accessible states, indicating some changes in the surface/structure of these CDs with the addition of the S-dopant. This is consistent with their light absorption data (Fig. 2C).

Microscopy, structural and surface characterization of CDs

After analyzing the optical properties of both CDs, it is important to perform their microscopy, structural and surface characterization. More specifically, the focus is on performing a comparative analysis to gain insight into the changes induced by co-S-doping and how they can account for the reduction in QY_{FL}.

AFM height analysis of the topography of both samples showed distinct and separated objects with sub-10 nm particle height (Fig. 6). This indicates that N-CDs and N,S-CDs possess a nanosize nature, consistent with the literature reports for CDs.[78–80]

The CDs were also studied by DLS at two different mass concentrations (0.06 and 0.14 g L^{-1}) (Fig. S3 and S4). Their hydrodynamic diameters and mean ζ potentials are presented in Table 1. Regarding the latter, we can see that N,S-CDs have higher ζ potentials at both concentrations and, therefore, should be more stable in solution (Fig. S3B).

DLS analysis of N-CDs and N,S-CDs at concentrations of 0.06 g L^{-1} and 0.14 g L^{-1} reveals significant differences in size distribution and aggregation behavior (Table 1 and Fig. S4).

The intensity-weighted data (Fig. S4A) indicate that at 0.06 g L^{-1}, N-CDs exhibit a bimodal distribution with peaks at approximately 0.3 μm and 14 μm. However, at 0.14 g L^{-1} (Fig. S4B), the bimodal distribution transitions to a single peak around 0.5 μm, accompanied by an increase in hydrodynamic diameter from 0.3949 μm at 0.06 g L^{-1} to 0.7199 μm at 0.14 g L^{-1}, suggesting increased aggregation at higher concentrations. In contrast, N,S-CDs exhibit a bimodal distribution at both concentrations, with peaks at approximately 0.2 μm and 5 μm at 0.06 g L^{-1}, and at approximately 0.2 μm and 14 μm at 0.14 g L^{-1}. The hydrodynamic diameter of N,S-CDs decreases from 0.3652 μm at 0.06 g L^{-1} to 0.2826 μm at 0.14 g L^{-1}, suggesting improved colloidal stability with increasing concen-

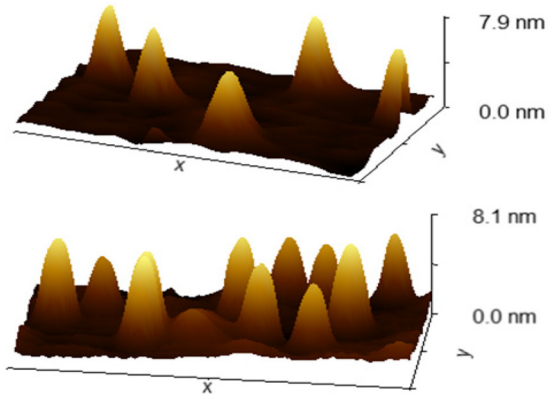

Fig. 6 AFM analysis of N-CDs (top) and N,S-CDs (bottom), showing representative 3D height images selected from full 10 × 10 μm (N-CDs) and 5 × 5 μm (N,S-CDs) scans. *Z*-Scale: 7.9 nm (N-CDs, top) and 8.1 nm (N,S-CDs, bottom).

Table 1 Results of DLS and ζ potential of N-CDs and N,S-CDs at different concentrations

CDs	Hydrodynamic diameter (μm)	Mean ζ potential (mV)
N-CDs 0.06 g L^{-1}	0.3949	−11.9
N-CDs 0.14 g L^{-1}	0.7199	−12.4
N,S-CDs 0.06 g L^{-1}	0.3652	−16.6
N,S-CDs 0.14 g L^{-1}	0.2826	−18.1

tration. The number-weighted distribution (Fig. S3A) further highlights key differences in particle size. At 0.06 g L^{-1}, N-CDs predominantly exhibit particle sizes with a peak at ≈0.07 μm, whereas at 0.14 g L^{-1}, the peak shifts to ≈0.03 μm, confirming a reduction in primary particle size with increasing concentration. In contrast, N,S-CDs maintain a relatively stable size distribution across both concentrations, with a consistent peak at 0.11 μm. These findings suggest that the tendency for aggregation is strongly dependent on particle composition, as N-CDs show a reduction in primary particle size with increasing concentration, whereas N,S-CDs maintain a stable size distribution, indicating higher colloidal stability. These differences in aggregation behavior for the CDs are in line with their respective mean ζ potentials.

Two additional topics should be addressed when discussing DLS data. One is that while the hydrodynamic diameters of the CDs (a few hundred nanometers) are significantly higher than the particle height estimated by AFM (sub-10 nm), this difference is actually in line with the literature.[81] That is, due to their functionalized surface, the particles are capable of interacting between themselves *via* hydrogen bonding and electrostatic interactions, leading to their aggregation in solution.[82]

Another noteworthy aspect is that the variation in hydrodynamic diameter with concentration (Table 1) indicates that N-CDs aggregate with increasing concentration, while N,S-CDs become less aggregated. However, despite this different behavior, Fig. S1A shows that the fluorescence of both CDs increases with concentration. Furthermore, the fluorescence increase is more pronounced for N-CDs, whereas their aggregation behavior would suggest the opposite. Given this, N-CDs appear to exhibit aggregation-induced emission behavior.[83,84] Meanwhile, co-S-doping decreased the aggregation potential of the CDs, which could be due to changes in surface functionalization of the nanoparticles. This is in line with the expected incorporation of additional functional groups in heteroatom-doping strategies and aligns with the data presented so far.

The XRD patterns of N-CDs and N,S-CDs are depicted in Fig. 7. In both XRD patterns, characteristic wide peaks near $2\theta \sim 25.0°$ (002 plane) and around 39.1° (100 planes) are observed, which reflect the presence of amorphous carbon.[85,86] The occurrence of oxygen-bearing functional groups that resemble amorphous carbon phases justifies this wide band.[87] The peak below 10.0° is ascribed to the (001) plane, to the presence of N and O groups and to the presence of organic compounds in the structure.[88] CDs having an amorphous nature are consistent with previous studies.[89–91]

EPR analysis of N-CDs and N,S-CDs (Fig. S5) did not reveal distinct peaks within the measured magnetic field range (2500 to 4500 G), indicating the absence of strongly detectable paramagnetic species. The lack of significant EPR signals suggests that unpaired electrons are either absent or present at concentrations too low to be detected under these conditions. This result highlights that the introduction of sulfur into the carbon dot structure does not induce notable paramagnetic behavior.

The CDs were also analyzed by FT-IR (Fig. 8), to gain valuable insights into how co-S-doping affects the functional groups present in the CDs. The obtained spectra are typical of doped CDs, with a broad band in the 2500–3500 cm^{-1} range, which demonstrates overlapping O–H and N–H stretching vibration modes.[12,28,92] Other relevant and common peaks can be found at ~1548/1557 cm^{-1} (N-CDs/N,S-CDs), ~1384 cm^{-1}, and ~1043/1039 cm^{-1} (N-CDs/N,S-CDs). According to previous studies, these peaks can be attributed to C=C/N–H, C–H/O–H, and C–O groups, respectively.[30,57,93–95]

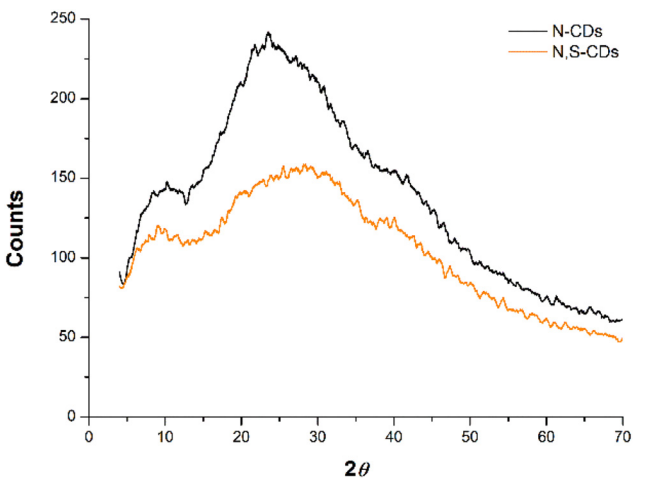

Fig. 7 XRD patterns of both CDs.

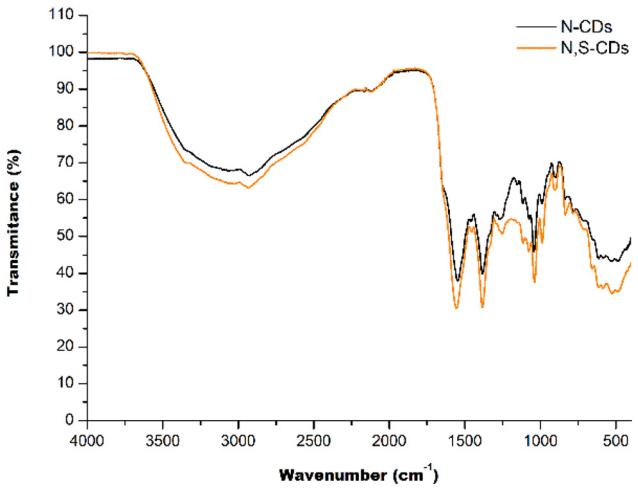

Fig. 8 FT-IR spectra of both CDs.

Given the use of an S-dopant to produce N,S-CDs, we would expect the presence of groups such as C–S, S–H, and O═S═O.[30,57,95–97] Some studies have indicated that C–S groups are associated with peaks at 690,[97] 713,[57] 1198 (ref. 30) and 1317 cm^{-1}.[95] S–H groups have been associated with bands at ~2500 cm^{-1},[97] while O═S═O with peaks between 1000 and 1180 cm^{-1} (1009, 1036, 1126, and 1176 cm^{-1}).[96] Unexpectedly, we did not find any particular peak in the FTIR spectrum of N, S-CDs that could be associated with S-based groups (Fig. 8), or that differed from what was found for N-CDs. In fact, the spectra of both CDs are quite identical in peak position and shape (Fig. 8), which indicates that the identity of the functional groups that they are composed of is very similar. Given this, the FTIR data suggest that despite the relevant effect that S-dopant addition had on the QY_{FL} of N,S-CDs, S-doping might not have been particularly efficient.

The surface composition of both CDs was investigated by XPS. The survey XPS results (Fig. S6) indicate that N-CDs are composed mainly of C (69.45%), O (19.26%), and N (11.30%). High-resolution spectra for the C 1*s*, N 1*s*, and O 1*s* levels were obtained for the N-CDs. To determine the functional groups on the surface of the CDs, the corresponding deconvolution, chemical state, and quantitative analyses were carried out. The C 1*s* spectrum of N-CDs (Fig. 9A) consists of four contributions: 284.5, 286.2, 287.9, and 289.32 eV. The produced graphitic structure carbon is responsible for the main contribution at 284.5 eV. The contributions at 286.2, 287.9, and 289.2 eV are due to the presence of C–O/C–N, C═O, and O–C═O groups, respectively. The N 1*s* spectrum (Fig. 9B) reveals three peaks, with their full width at half maximum (FWHM) values given in parentheses: 398.4 (1.85), 399.4(2), and 401.0 eV (2), which are ascribed to the pyridinic, pyrrolic, and quaternary N atoms, respectively.[98] The O 1*s* spectrum showed two contributions at 531.2 eV (C═O) and 532.8 eV (C–O) (Fig. 9C).

The survey XPS results reveal that N,S-CDs are superficially composed of C (63.70%), O (21.82%), N (10.14%), and S (1.67%), respectively, as shown in the full-scan spectrum (Fig. S6). The deconvoluted C 1*s* spectrum (Fig. 9D) shows three peaks: at 284.8 eV, attributed to C═C/C–C; at 285.9 eV, attributed to C–O/C–N/C–S; at 287.6 eV, attributed to C═O groups. The N 1*s* spectrum (Fig. 9E) showed a complex of 4 different contributions: 398.5 eV (2.7), 399.96 eV (1.97), 401.52 eV (2.03), and 402.5 eV (2.29), corresponding to pyridinic N, pyrrolic N, quaternary N, and oxidized N, respectively. The O 1*s* spectrum showed three contributions at 531, 532.6, and

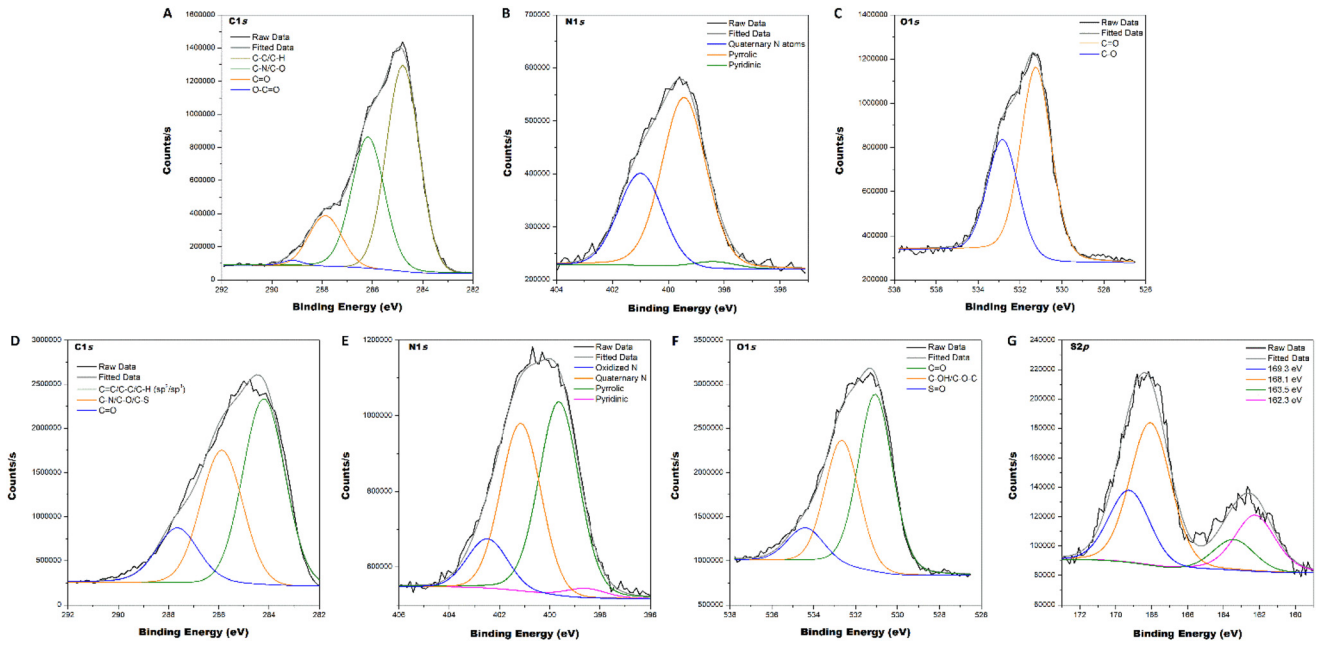

Fig. 9 XPS core-level spectra of N-CDs: C 1*s* (A), N 1*s* (B), and O 1*s* (C); and of N,S-CDs: C 1*s* (D), N 1*s* (E), O 1*s* (F), and S 2*p* (G).

534.4 eV, which are assigned to C=O, C–OH/C–O–C, and O–C/O–S bonds (Fig. 9F).[99] The S 2*p* spectrum is shown in Fig. 9G and consists of two distinct doublets: one at 162.3/163.5 eV and the other at 168.1/169.3 eV. The former is indicative of reduced sulfur species, such as thiophene-like or sulfide groups. The latter is characteristic of oxidized sulfur forms, such as C-SO_X groups. This spectrum is consistent with that observed for S-doped CDs. However, the higher intensity of the 168.1/169.3 eV doublet and the presence of a Na signal in the XPS survey (Fig. S6) could also indicate the presence of residual thiosulfate.

Postulated mechanism for QY_{FL}-reduction

Consistent with FTIR, the XPS results reveal that S surface incorporation is residual and that the main compositional difference between N-CDs and N,S-CDs lies in surface oxidation rather than S content. Specifically, N,S-CDs exhibit a lower C content (~64% *vs.* ~70%) and a higher O content (22% *vs.* ~19%), which corresponds to an ~24% increase in the O : C ratio (from 0.27 to 0.34). Meanwhile, the S content was below 2%, despite the addition of $Na_2S_2O_3$ in a 1 : 1 : 1 mass ratio with the N-dopant and the combined carbon precursors. This indicates that $Na_2S_2O_3$ did not act as an effective dopant under the employed conditions.

This last finding is surprising given the marked decrease of QY_{FL} observed for N,S-CDs (by 63%), which appears to be too large a variation to be caused by such residual co-S-doping. Nevertheless, the low S ratio in N,S-CDs helps explain why their optical properties (besides QY_{FL}) are quite similar to those of N-CDs.

As stated in the Introduction section, while different researchers have claimed that heteroatom doping has some QY_{FL}-changing properties,[24,26,35–38] it is still not proven that the measured effects are truly due to the inclusion of those heteroatoms.[4,39–41] Given this, it is possible that the QY_{FL} decrease is not due to the (residual) S-doping here achieved.

Nevertheless, any difference between N-CDs and N,S-CDs results, in a way or another, from the inclusion of $Na_2S_2O_3$ in the synthesis mixture of the latter.

Repeated syntheses of N,S-CDs consistently produced a "rotten-egg" odor upon opening the hydrothermal reactor, suggesting the release of reduced sulfur species.[100] This observation, together with previous reports of $Na_2S_2O_3$ decomposition and disproportionation in aqueous solutions under heating,[101–104] indicates that this compound was not inert but chemically transformed during the reaction. Thus, the measured compositional changes between N-CDs and N,S-CDs are most likely due to (secondary) redox effects arising from thiosulfate decomposition, rather than surface S-doping.

In fact, the observed increase in the O : C ratio in XPS demonstrates that $Na_2S_2O_3$ addition promoted surface oxidation of the CDs, producing a more oxygenated material. This was achieved while the CDs maintained an identical N : C ratio of ~0.16. Consequently, the N,S-CDs here obtained can be interpreted as oxidized N-CDs rather than as true co-doped nanomaterials. Interestingly, this oxidant-like role of $Na_2S_2O_3$ was described before.[105]

Finally, the observation that N,S-CDs are more akin to an oxidized version of N-CDs, rather than an actual co-doped nanomaterial, helps to explain the measured QY_{FL} reduction. Specifically, Chahal *et al.*[41] have claimed that QY_{FL} is correlated with the O : C ratio and that N-doping is insufficient to increase QY_{FL}. This is in line with our data, as the N : C ratio difference between N-CDs and N,S-CDs is negligible, while the latter nanoparticles are more oxidized than the former (O : C ratio is increased by ~24%). Previous authors have also correlated lower QY_{FL} with higher oxidation degrees.[106,107] This can be explained by the formation of oxygen-based surface defects that act as non-radiative centers, thereby allowing for non-radiative relaxation pathways.[108,109] This is compatible with our data, especially considering the fact that despite the QY_{FL} being markedly lower in N,S-CDs, their emission band position and shape remained mainly unchanged (when compared with N-CDs). Furthermore, the fluorescence of N,S-CDs presented a similar variation to external media/stimuli as N-CDs, with some apparent contribution from more surface-accessible states.

It should be noted that the potential presence of residual thiosulfate (Fig. 9G and S6) could raise the question of whether the QY_{FL} decrease could be attributed to it instead (by quenching effects). To investigate this, we measured the potential quenching effect of $Na_2S_2O_3$ toward N-CDs and N,S-CDs, at quencher concentrations up to 100 mM (Fig. S8). The quenching effect was found to range from negligible to small. Specifically, at 30 mM, the F_0/F ratio for N-CDs was still ~1 and just ~1.20 for N,S-CDs. These small effects are unlikely to account for the observed 63% decrease in QY_{FL}, especially given that the residual concentration of potential thiosulfate should be significantly lower than the range investigated here (mM levels). Finally, it should also be said that even if residual thiosulfate is present, it still supports our conclusion that $Na_2S_2O_3$ did not act as an effective dopant under these conditions.

To better assess the extension of our conclusions, we also synthesized two additional CDs: N,S-$CDs_{thiourea}$ and N,S-CDs_{half}. The former was produced in the same way as N,S-CDs, except that $Na_2S_2O_3$ was replaced with thiourea. N,S-CDs_{half} were produced with $Na_2S_2O_3$ but in a 1 : 1 : 0.5 mass ratio (C, N and S sources, respectively), that is, half the amount of $Na_2S_2O_3$ used to produce N,S-CDs. Their EECPs are shown in Fig. S9, and their QYs_{FL} are 3.8% (N,S-$CDs_{thiourea}$) and 34.1% (N,S-CDs_{half}).

This shows that the use of thiourea has also resulted in a significant decrease in QY_{FL} (by 89%), when compared with N-CDs. This indicates that the detrimental effect attributed to the S-precursors is not limited to $Na_2S_2O_3$. Regarding N,S-CDs_{half}, their QY_{FL} is actually similar to that of N-CDs (5% decrease). This indicates that the detrimental effect of $Na_2S_2O_3$ is concentration-dependent, which is expected for redox/surface-modification routes. Furthermore, while similar, the QY_{FL} is still inferior to that of N-CDs. Thus, it is another

example where co-S-doping does not provide a visible performance enhancement over N-doped CDs.

Overall, our data show that the co-addition of $Na_2S_2O_3$ during hydrothermal synthesis does not lead to effective S surface incorporation but instead promotes oxidation of the carbon surface. The resulting N,S-CDs are therefore best described as oxidized N-CDs with a higher O : C ratio, where oxygen-based surface traps are hypothesized to account for the observed 63% decrease in quantum yield. This finding highlights the possibility that some S-precursors commonly used for S-doping may act primarily as redox modifiers rather than dopants, emphasizing the need for careful surface-composition correlation when interpreting QY_{FL} changes in doped CDs.

Beyond this specific case, our results may reveal a broader issue in CD research. While many studies attribute optical property modulation to heteroatom doping, in the field there is a limited quantitative assessment of heteroatom incorporation into CDs and how it correlates with the observed changes. Given this, the role of "dopants" may be misinterpreted, and non-doping surface oxidation/modification effects may be overlooked. Compounds intended as dopants may in fact act primarily as redox-active agents, catalysts, or surface modifiers. Hence, there is a need for systematic compositional analysis and mechanistic validation when evaluating the true impact of doping strategies on CD emission. Nevertheless, it should be noted that our work focused solely on hydrothermal reactions and not on other synthesis routes (such as microwave-assisted or dry-heating). It was also focused on $Na_2S_2O_3$ rather than other common S-precursors (such as cysteine). Therefore, future work is needed to properly assess the impact of our results in the field of CDs.

Experimental

Carbon dot synthesis procedures

N-CDs and N,S-CDs were produced by following a general hydrothermal treatment route previously developed by us for the synthesis of brightly emissive waste-based CDs.[12] Specifically, the precursor mixtures for both CDs were prepared in a NaOH (0.01 M) solution, with the final reaction volume being 10 mL. For N-CDs, the precursor mixture consisted of the carbon precursors citric acid and sawdust (the waste material), in a 50 : 50 mass ratio (total 0.15 g), and the N-dopant (EDA, 0.15 g). N,S-CDs were prepared from a similar mixture, with the difference being the addition of also 0.15 g of $Na_2S_2O_3$ pentahydrate as an S-dopant. Both reaction mixtures were placed in a 25 mL Teflon-lined reactor with a stainless-steel shell from Cambridge Energy Solutions (CES) and then heated at 200 °C for 8 h in a D-6450 Hanau oven from Heraeus. Afterwards, the resulting CD solutions were placed in an ultrasonic bath from VWR, model USC100TH, for 20 minutes. Later, the samples were centrifuged for 30 minutes at 6000 rpm through a MIKRO 220R from Hettich to remove suspended particles. The precipitate was discarded, and the supernatant was further purified. The CDs were subsequently subjected to dialysis for 24 hours, using a Float-A-Lyzer®G2 dialysis device, MWCO: 3500 Da. The commercial chemicals used in the synthesis were citric acid anhydrous (>99%), EDA (≥99%), and NaOH (≥97%) from Sigma-Aldrich, as well as $Na_2S_2O_3$ from Merck. The sawdust was supplied by a Portuguese company specializing in timber trading and the production of derivative products. The efficiency of the dialysis process was assessed by measuring the absorbance of the dialysate solutions at 350 nm (the excitation wavelength of the CDs), at the first cycle of water replacement and at the end of the 24 h dialysis (Fig. S7). While the absorbance at the end of the first cycle was 0.116–0.123, at 24 h, only basal absorbance values were observed for both CDs (0.003–0.007). These decreases correspond to almost 100% (~95% for N-CDs and ~97% for N,S-CDs) and support the adequacy of our dialysis conditions.

Characterization techniques

Fluorescence measurements were performed using a Horiba Jobin Yvon Fluoromax-4 spectrofluorometer, using a standard 10 mm fluorescence quartz cell. The fluorescence spectra were acquired with slit widths set to 2 nm. Samples were analyzed at a fixed concentration of 0.1 g L^{-1}, except in concentration-dependent assays. Absorbance spectra were recorded using a UV-3100PC spectrophotometer from VWR, using quartz cells.

Dynamic light scattering (DLS) and ζ-potential measurements were conducted using an Anton Paar Litesizer™ 500 particle analyzer. ζ-Potential measurements were performed using a polycarbonate Omega cuvette, and size measurements (by DLS) were carried out using a disposable polystyrene cuvette.

Fourier transform infrared (FT-IR) spectroscopy was conducted using a PerkinElmer Spectrum Two FT-IR spectrometer (ATR module) and Spectrum software. The analysis included 4 scans per spectrum and covered a wavenumber range from 4000 to 400 cm^{-1}.

Using monochromatic Al-K_α radiation (49.1 W, 15 kV, and 1486.6 eV), X-ray photoelectron spectroscopy (XPS) was conducted on a Physical Electronics PHI VersaProbe II spectrometer to analyze the core-level signals of the components of interest using a hemispherical multichannel detector. Over a circular analysis region of 200 μm in diameter, the sample spectra were recorded with a constant pass energy value of 29.35 eV. PHI SmartSoft software was used to analyze the acquired XPS spectra, and MultiPak 9.3 was used for processing. The adventitious carbon C 1*s* signal (284.8 eV) served as the reference for the binding energy measurements. The binding energies were found using Gaussian-Lorentzian curves and Shirley-type backgrounds.

Laboratory X-ray powder diffraction (XRPD) patterns were collected using a PANalytical EMPYREAN automated diffractometer. Powder patterns were recorded in Bragg–Brentano reflection configuration by using a PIXcel 3D detector with a step size of 0.01° (2θ). The powder patterns were recorded between 5 and 70 in 2θ with a total measurement time of 60 min.

Electron paramagnetic resonance (EPR) spectra were recorded using a Bruker Elexys III E580 spectrometer, which operates in the X-band (9.5 GHz).

Atomic force microscopy (AFM) analysis was conducted with a Nano-Observer AFM (CSInstruments AFM Microscopes, Les Ulis, France). For this purpose, a mica substrate treated with 0.01% poly-L-lysine hydrobromide was used to deposit the sample, and measurements were carried out using a sharp Si N-type probe with a resistance of 0.01–0.025 Ω cm and a resonance frequency of 200–400 kHz. Samples were prepared by drop evaporation of a diluted CD solution, and Gwyddion software was used for AFM data analysis.

Fluorescence quantum yield

The fluorescence quantum yield (QY_{FL}) was determined following a standard methodology, which involves comparing the integrated luminescence intensities and absorbance values of the sample (in this case, the CDs) to those of a reference fluorophore, quinine sulfate (QS). The calculation of QY_{FL} is based on the following equation,

$$QY_{FL} = QY_{FL_{QS}} \times \frac{Grad_{sample}}{Grad_{QS}} \times \frac{\eta_{sample}{}^2}{\eta_{QS}{}^2} \times 100$$

where "Grad" represents the gradient derived from the plot of integrated fluorescence intensity *versus* absorbance and "η" denotes the refractive index.

In this study, QS was utilized as the reference fluorophore due to its established QY_{FL} of 0.54. QS is commonly used for QY_{FL} determination of CDs because it absorbs at the selected excitation wavelength and emits in a spectral region comparable to that of typical CDs, including the ones analyzed in this study. The refractive index of the reference (QS) was 1.33 (0.1 M H_2SO_4), and the sample (CDs) was 1.34 (H_2O). To minimize reabsorption effects, the absorbance at the excitation wavelength was kept below 0.1.

Conclusions

In summary, this study provided a comprehensive and comparative characterization of N-CDs and N,S-CDs synthesized from sawdust, citric acid, EDA, and $Na_2S_2O_3$ under hydrothermal conditions. More specifically, while heteroatom-doping strategies are widely used to enhance the QY_{FL} of CDs, there is a limited understanding of the mechanism behind it. In fact, it is still unclear how truly effective these strategies are. One example is the lack of a comprehensive demonstration that co-N,S-doping provides additional advantages over single N-doping approaches. Herein, our study aimed to provide insight into these processes by focusing on commonly used precursors, N- and S-dopants, and synthesis strategies, thereby ensuring a broader generalization of the conclusions within this research field.

Despite the broadly claimed benefits of co-N,S-doping and the common use of $Na_2S_2O_3$ as an S-dopant, the results revealed that its inclusion markedly reduced the QY_{FL} of N,S-CDs by 63%. Detailed microscopic and spectroscopic analyses indicate that this loss in QY_{FL} is not due to successful S-doping, but rather to a more oxidized surface, as evidenced by the higher O : C ratio measured by XPS. These findings suggest that the inclusion of $Na_2S_2O_3$ had a primarily oxidizing effect during the synthesis rather than the compound acting as a dopant, promoting oxygen-based surface defects that introduce nonradiative traps. In other words, the addition of $Na_2S_2O_3$ resulted in more oxidized N-CDs rather than co-doped N,S-CDs. It should be noted that thiourea was also found to cause a marked reduction in QY_{FL}.

Beyond this specific case, this study highlights the possibility that heteroatom-containing compounds can behave as redox-active modifiers rather than true dopants. As such, future studies should perform more quantitative assessments and validation of heteroatom incorporation into the resulting CDs, to better distinguish between real doping effects and surface modifications mediated by heteroatom-based compounds. Furthermore, S-precursors (*e.g.*, cysteine), which are also commonly used, should be specifically investigated to assess whether they induce this QY_{FL}-reducing effect, at least under some experimental conditions. Thus, this study provides valuable insight into the use of heteroatom precursors, which can inform a more rational design of better-performing CDs.

Author contributions

Conceptualization: LPS; investigation: SF, MA, and AB; visualization: SF and MA; supervision: LPS, JES, and CMP; funding acquisition: LPS, CMP, JES, and MA; writing – original draft: SF and MA; and writing – revision: LPS, MA, AG, AB, CMP, and JES.

Conflicts of interest

There are no conflicts to declare.

Data availability

The data supporting this article have been included as part of the supplementary information (SI). Supplementary information: emission intensity *vs* absorbance, photostability and ET(30) assays, DLS number- and intensity-weighted size distributions, EPR assay, XPS survey spectra, dialysis absorbance data of the external solution (350 nm) after 24h purification for both CDs, Stern-Volmer plots for the potential quenching effect of Na_2S_{23}, and EECPs of N,S-CDs_{half} and N,S-$CDs_{thiourea}$. See DOI: https://doi.org/10.1039/d5nr05082k.

Acknowledgements

"Fundação para a Ciência e a Tecnologia" (FCT, Portugal, https://ror.org/00snfqn58) is acknowledged for funding the

R&D Unit CIQUP (UID/00081/2025), project 2023.13127.PEX and the Associated Laboratory IMS (LA/P/0056/2020). The NORTE2030 program is also acknowledged for funding the project NORTE2030-FEDER-02706400 (iChem4M). Luís Pinto da Silva acknowledges funding from the FCT under the Scientific Employment Stimulus (CEECINST/00069/2021). Sónia Fernandes also acknowledges the FCT for funding her Ph.D. grant (2021.05479.BD). For the purpose of Open Access, the authors have applied a CC-BY public copyright license to any Author Accepted Manuscript (AAM) version arising from this submission. The authors also acknowledge the Lab&Services of the Chemistry and Biochemistry Department of the Faculty of Sciences of Porto University (FCUP|DQB – Lab&Services) and CEMUP (Materials Centre of the University of Porto). Manuel Algarra thanks the projects MCIN/AEI/10.13039/501100011033 and PID2021-122613OB-I00.

References

1 S. Dua, P. Kumar, B. Pani, A. Kaur, M. Khanna and G. Bhatt, *RSC Adv.*, 2023, **13**(20), 13845–13861, DOI: 10.1039/d2ra07180k.
2 J. Liu, R. Li and B. Yang, *ACS Cent. Sci.*, 2020, **6**(12), 2179–2195, DOI: 10.1021/acscentsci.0c01306.
3 R. M. S. Sendão, J. C. G. Esteves da Silva and L. Pinto da Silva, *Chemosphere*, 2022, **301**, 134731, DOI: 10.1016/j.chemosphere.2022.134731.
4 D. Crista, M. Algarra, M. V. Martínez de Yuso, J. C. G. Esteves da Silva and L. Pinto da Silva, *J. Mater. Chem. B*, 2023, **11**(5), 1131–1143, DOI: 10.1039/d2tb02318k.
5 G. Rodríguez-Carballo, R. Moreno-Tost, S. Fernandes, J. C. G. Esteves da Silva, L. Pinto da Silva, E. C. Galiano and M. Algarra, *J. Cleaner Prod.*, 2023, **423**, 138728, DOI: 10.1016/j.jclepro.2023.138728.
6 C. M. Magalhães, E. Ribeiro, S. Fernandes, J. C. G. Esteves da Silva, N. Vale and L. Pinto da Silva, *Cancers*, 2024, **16**(19), 3332, DOI: 10.3390/cancers16193332.
7 Y. Wang and A. Hu, *J. Mater. Chem. C*, 2014, **2**(34), 6921, DOI: 10.1039/c4tc00988f.
8 A. Bafana, S. V. Kumar, S. Temizel-Sekeryan, S. A. Dahoumane, L. Haselbach and C. S. Jeffryes, *Sci. Total Environ.*, 2018, **636**, 936–943, DOI: 10.1016/j.scitotenv.2018.04.345.
9 M. J. Eckelman, J. B. Zimmerman and P. T. Anastas, *J. Ind. Ecol.*, 2008, **12**(3), 316–328, DOI: 10.1111/j.1530-9290.2008.00043.x.
10 S. Fernandes, J. C. G. Esteves da Silva and L. Pinto da Silva, *NanoImpact*, 2021, **23**, 100332, DOI: 10.1016/j.impact.2021.100332.
11 L. Pourzahedi and M. J. Eckelman, *Environ. Sci.:Nano*, 2015, **2**(4), 361–369, DOI: 10.1039/c5en00075k.
12 S. Fernandes, M. Algarra, A. Gil, J. C. G. Esteves da Silva and L. Pinto da Silva, *ChemSusChem*, 2025, **18**(2), e202401702, DOI: 10.1002/cssc.202401702.
13 A. Johny, L. Pinto da Silva, C. M. Pereira and J. C. G. Esteves da Silva, *Environments*, 2024, **11**(1), 6, DOI: 10.3390/environments11010006.
14 D. M. A. Crista, A. El Mragui, M. Algarra, J. C. G. Esteves da Silva, R. Luque and L. Pinto da Silva, *Nanomaterials*, 2020, **10**(6), 1316, DOI: 10.3390/nano10061209.
15 F. Aldakhil, N. A. Alarfaj, S. A. Al-Tamimi and M. F. El-Tohamy, *RSC Adv.*, 2024, **14**(28), 19969–19982, DOI: 10.1039/d4ra02398f.
16 S. Zhu, Y. Song, X. Zhao, J. Shao, J. Zhang and B. Yang, *Nano Res.*, 2015, **8**(2), 355–381, DOI: 10.1007/s12274-014-0644-3.
17 C. Kang, Y. Huang, H. Yang, X. F. Yan and Z. P. Chen, *Nanomaterials*, 2020, **10**(11), 2316, DOI: 10.3390/nano10112316.
18 J. R. Bhamore, S. Jha, R. K. Singhal, T. J. Park and S. K. Kailasa, *J. Mol. Liq.*, 2018, **264**, 9–16, DOI: 10.1016/j.molliq.2018.05.041.
19 R. Atchudan, T. N. J. I. Edison, D. Chakradhar, S. Perumal, J.-J. Shim and Y. R. Lee, *Sens. Actuators, B*, 2017, **246**, 497–509, DOI: 10.1016/j.snb.2017.02.119.
20 A. M. Senol and E. Bozkurt, *Microchem. J.*, 2020, **159**, 105357, DOI: 10.1016/j.microc.2020.105357.
21 Q. Xu, P. Pu, J. Zhao, C. Dong, C. Gao, Y. Chen, J. Chen, Y. Liu and H. Zhou, *J. Mater. Chem. A*, 2015, **3**(2), 542–546, DOI: 10.1039/c4ta05483k.
22 C. Wang, Y. Wang, H. Shi, Y. Yan, E. Liu, X. Hu and J. Fan, *Mater. Chem. Phys.*, 2019, **232**, 145–151, DOI: 10.1016/j.matchemphys.2019.04.071.
23 Q. Xu, J. Zhao, Y. Liu, P. Pu, X. Wang, Y. Chen, C. Gao, J. Chen and H. Zhou, *J. Mater. Sci.*, 2015, **50**(6), 2571–2576, DOI: 10.1007/s10853-015-8822-6.
24 G. Somaraj, S. Mathew, T. Abraham, K. G. Ambady, C. Mohan and B. Mathew, *ChemistrySelect*, 2022, **7**(19), e202200473, DOI: 10.1002/slct.202200473.
25 A. Nasrin, M. Hassan, G. Mann and V. G. Gomes, *J. Lumin.*, 2020, **217**, 116811, DOI: 10.1016/j.jlumin.2019.116811.
26 M. L. Liu, B. B. Chen, C. M. Li and C. Z. Huang, *Green Chem.*, 2019, **21**(3), 449–471, DOI: 10.1039/c8gc02736f.
27 H. Qi, L. Qiu, X. Zhang, T. Yi, J. Jing, R. Sami, S. F. Alanazi, Z. Alqahtani, M. D. Aljabri and M. M. Rahman, *RSC Adv.*, 2023, **13**(4), 2663–2671, DOI: 10.1039/d2ra07150a.
28 T. T. A. Do, K. Wicaksono, A. Soendoro, T. Imae, M. J. Garcia-Celma and S. Grijalvo, *J. Funct. Biomater.*, 2022, **13**(4), 219, DOI: 10.3390/jfb13040219.
29 H. Song, Y. Li, L. Shang, Z. Tang, T. Zhang and S. Lu, *Nano Energy*, 2020, **72**, 104730, DOI: 10.1016/j.nanoen.2020.104730.
30 A. G. Kolekar, S. P. Pawar, D. B. Gunjal, O. S. Nille, P. V. Anbhule, S. V. Koparde, N. Q. Nguyen, D. Sohn, G. B. Kolekar, G. S. Gokavi and V. R. More, *RSC Adv.*, 2024, **14**(5), 3473–3479, DOI: 10.1039/d3ra07545a.
31 H. Wang, W. Mu, S. Wang, L. Shi, T. Ma and Y. Lu, *Spectrochim. Acta, Part A*, 2024, **305**, 123460, DOI: 10.1016/j.saa.2023.123460.

32 C. Cheng, M. Xing and Q. Wu, *Mater. Sci. Eng., C*, 2019, **99**, 611–619, DOI: 10.1016/j.msec.2019.02.003.
33 Y. Venkatesh, P. V. S. Naidu, M. Ramanjaneyulu, P. A. Rao and D. B. Kundrapu, *J. Nanopart. Res.*, 2025, **27**(3), 62, DOI: 10.1007/s11051-025-06260-y.
34 A. Saengsrichan, C. Saikate, P. Silasana, P. Khemthong, W. Wanmolee, J. Phanthasri, S. Youngjan, P. Posoknistakul, S. Ratchahat, N. Laosiripojana, K. C. Wu and C. Sakdaronnarong, *Int. J. Mol. Sci.*, 2022, **23**(9), 5001, DOI: 10.3390/ijms23095001.
35 Y. Li, Y. Zhao, H. Cheng, Y. Hu, G. Shi, L. Dai and L. Qu, *J. Am. Chem. Soc.*, 2012, **134**(1), 15–18, DOI: 10.1021/ja206030c.
36 M. Yang, X. Meng, B. Li, S. Ge and Y. Lu, *J. Nanopart. Res.*, 2017, **19**(6), 217, DOI: 10.1007/s11051-017-3914-7.
37 D. Qu, M. Zheng, L. Zhang, H. Zhao, Z. Xie, X. Jing, R. E. Haddad, H. Fan and Z. Sun, *Sci. Rep.*, 2014, **4**, 5294, DOI: 10.1038/srep05294.
38 W. Zou, J. Li and X. Gong, *Mater. Today Chem.*, 2024, **37**, 102001, DOI: 10.1016/j.mtchem.2024.102001.
39 D. M. A. Crista, J. C. G. Esteves da Silva and L. Pinto da Silva, *Nanomaterials*, 2020, **10**(7), 1316, DOI: 10.3390/nano10071316.
40 S. Christe, J. C. G. Esteves da Silva and L. Pinto da Silva, *Materials*, 2020, **13**(3), 504, DOI: 10.3390/ma13030504.
41 S. Chahal, N. Yousefi and N. Tufenkji, *ACS Sustainable Chem. Eng.*, 2020, **8**(14), 5566–5575, DOI: 10.1021/acssuschemeng.9b07463.
42 Z. Yi, X. Li, H. Zhang, X. Ji, W. Sun, Y. Yu, Y. Liu, J. Huang, Z. Sarshar and M. Sain, *Talanta*, 2021, **222**, 121663, DOI: 10.1016/j.talanta.2020.121663.
43 Y. Liu, L. Jiang, B. Li, X. Fan, W. Wang, P. Liu, S. Xu and X. Luo, *J. Mater. Chem. B*, 2019, **7**(19), 3053–3058, DOI: 10.1039/c9tb00021f.
44 J. B. Essner, J. A. Kist, L. Polo-Parada and G. A. Baker, *Chem. Mater.*, 2018, **30**(6), 1878–1887, DOI: 10.1021/acs.chemmater.7b04446.
45 N. Ullal, R. Mehta and D. Sunil, *Analyst*, 2024, **149**(6), 1680–1700, DOI: 10.1039/d3an02134c.
46 D. A. Sousa, M. N. Berberan-Santos and J. V. Prata, *Chemistry*, 2024, **30**(3), e202302955, DOI: 10.1002/chem.202302955.
47 Y. Hu, O. Seivert, Y. Tang, H. E. Karahan and A. Bianco, *Angew. Chem., Int. Ed.*, 2024, **63**(48), e202412341, DOI: 10.1002/anie.202412341.
48 H. Li, J. Xiao, J. Cao, J. Pan, C. Li and Y. Zheng, *J. Nanopart. Res.*, 2025, **27**(5), 140, DOI: 10.1007/s11051-025-06332-z.
49 P. Liu, C. Zhang, X. Liu and P. Cui, *Appl. Surf. Sci.*, 2016, **368**, 122–128, DOI: 10.1016/j.apsusc.2016.01.278.
50 J. Zheng, Y. Xie, Y. Wei, Y. Yang, X. Liu, Y. Chen and B. Xu, *Nanomaterials*, 2020, **10**(1), 82, DOI: 10.3390/nano10010082.
51 A. Abdel-Hakim, F. Belal, M. A. Hammad and M. El-Maghrabey, *Methods Appl. Fluoresc.*, 2023, **11**(4), 045007, DOI: 10.1088/2050-6120/acf119.
52 H. P. Dang, V. T. N. Thuy, B. T. Diem, N. Q. Thang and N. T. M. Tho, *Opt. Quantum Electron.*, 2025, **57**(5), 291, DOI: 10.1007/s11082-025-08185-1.
53 Q. Xu, Y. Liu, C. Gao, J. Wei, H. Zhou, Y. Chen, C. Dong, T. S. Sreeprasad, N. Li and Z. Xia, *J. Mater. Chem. C*, 2015, **3**(38), 9885–9893, DOI: 10.1039/c5tc01912e.
54 D. Qu, M. Zheng, P. Du, Y. Zhou, L. Zhang, D. Li, H. Tan, Z. Zhao, Z. Xie and Z. Sun, *Nanoscale*, 2013, **5**(24), 12272–12277, DOI: 10.1039/c3nr04402e.
55 S. Chen, W. Ouyang, Y. Zhu, L. He, L. Zou, X. Ao, S. Liu, Y. Yang and J. Li, *Foods*, 2022, **11**(16), 2414, DOI: 10.3390/foods11162414.
56 R. Tamizhselvi, K. S. Velu, A. A. Napoleon, M. S. Akhtar, N. Ahmad, S. Palanisamy, S. You, S. Mohandoss and S.-C. Kim, *Inorg. Chem. Commun.*, 2025, **172**, 113662, DOI: 10.1016/j.inoche.2024.113662.
57 O. A. Aladesuyi and O. S. Oluwafemi, *Inorg. Chem. Commun.*, 2023, **153**, 110843, DOI: 10.1016/j.inoche.2023.110843.
58 M. Hamid, S. Humaidi, H. Wijoyo, I. Isnaeni, I. R. Saragi, C. Simanjuntak, N. H. M. Kaus, M. M. A. Kechik, A. Nurbillah, Y. Yaakob and T. I. Nasution, *Case Stud. Chem. Environ. Eng.*, 2024, **10**, 100832, DOI: 10.1016/j.cscee.2024.100832.
59 J. Wang, Z. Wu, S. Chen, R. Yuan and L. Dong, *Microchem. J.*, 2019, **151**, 104246, DOI: 10.1016/j.microc.2019.104246.
60 J. Zhang, Z. Xu, C. Shi and X. Yang, *Sustainability*, 2021, **13**(15), 8255, DOI: 10.3390/su13158255.
61 H. K. M. Ng, G. K. Lim and C. P. Leo, *Microchem. J.*, 2021, **165**, 106116, DOI: 10.1016/j.microc.2021.106116.
62 A. O. Aswathy, S. M. Anju, J. Jayakrishna, N. S. Vijila, J. S. Anjali Devi, B. Anjitha and S. George, *J. Fluoresc.*, 2020, **30**(6), 1337–1344, DOI: 10.1007/s10895-020-02607-x.
63 S. R. Kamali, C.-N. Chen, D. C. Agrawal and T.-H. Wei, *J. Anal. Sci. Technol.*, 2021, **12**(1), 48, DOI: 10.1186/s40543-021-00298-y.
64 J. Guo, L. Fan, Q. Zan, J. Wang, Z. Yang, W. Lu, Y. Yang, X. Yang, C. Dong and S. Shuang, *Anal. Chem.*, 2023, **95**(32), 12139–12151, DOI: 10.1021/acs.analchem.3c02381.
65 V. I. Stsiapura, A. A. Maskevich, V. A. Kuzmitsky, V. N. Uversky, I. M. Kuznetsova and K. K. Turoverov, *J. Phys. Chem. B*, 2008, **112**(49), 15893–15902, DOI: 10.1021/jp805822c.
66 A. Neerkattil, M. M. Bijeesh, K. K. Ghosh, P. Padmanabhan, B. Gulyas, V. M. Murukeshan and J. Bhattacharyya, *Nanoscale Adv.*, 2025, **7**(9), 2686–2694, DOI: 10.1039/d5na00061k.
67 A. Chmyrov, T. Sanden and J. Widengren, *J. Phys. Chem. B*, 2010, **114**(34), 11282–11291, DOI: 10.1021/jp103837f.
68 K. E. Guðmundsson, G. Marteinsdóttir, K. Kristbergsson and Á. Kvaran, *Chem. Pap.*, 2022, **76**(8), 5253–5265, DOI: 10.1007/s11696-022-02222-z.
69 R. M. S. Sendão, M. Algarra, J. Lázaro-Martínez, A. T. S. C. Brandão, A. Gil, C. Pereira, J. C. G. Esteves da Silva and L. Pinto da Silva, *Colloids Surf., A*, 2025, **713**, 36475, DOI: 10.1016/j.colsurfa.2025.136475.
70 R. M. S. Sendão, M. Algarra, E. Ribeiro, M. Pereira, A. Gil, N. Vale, J. C. G. Esteves da Silva and L. Pinto da Silva, *Adv.*

Sustainable Syst., 2023, **8**(1), 2300317, DOI: 10.1002/adsu.202300317.
71 Y.-C. Wang, F. Zhu, J.-Y. Zhang and T.-M. Geng, *Microchem. J.*, 2025, **209**, 112739, DOI: 10.1016/j.microc.2025.112739.
72 J. Cao, X. An and S. Han, *Colloids Surf., A*, 2020, **586**, 124201, DOI: 10.1016/j.colsurfa.2019.124201.
73 Y. Song, S. Zhu, S. Xiang, X. Zhao, J. Zhang, H. Zhang, Y. Fu and B. Yang, *Nanoscale*, 2014, **6**(9), 4676–4682, DOI: 10.1039/c4nr00029c.
74 X. Ren, L. Guan, W. Shi, J. Zhang, M. Chen, T. Luo, C. Liu, Y. Lan, Z. Chen, X. Chen and X. Li, *J. Mol. Liq.*, 2024, **403**, 124872, DOI: 10.1016/j.molliq.2024.124872.
75 A. Das, D. Roy, C. K. De and P. K. Mandal, *Phys. Chem. Chem. Phys.*, 2018, **20**(4), 2251–2259, DOI: 10.1039/c7cp07411e.
76 J. Ren, F. Weber, F. Weigert, Y. Wang, S. Choudhury, J. Xiao, I. Lauermann, U. Resch-Genger, A. Bande and T. Petit, *Nanoscale*, 2019, **11**(4), 2056–2064, DOI: 10.1039/c8nr08595a.
77 P. K. Sarswat and M. L. Free, *Phys. Chem. Chem. Phys.*, 2015, **17**(41), 27642–27652, DOI: 10.1039/c5cp04782j.
78 A. Ventrella, A. Camisasca, A. Fontana and S. Giordani, *RSC Adv.*, 2020, **10**(60), 36404–36412, DOI: 10.1039/d0ra06172g.
79 F. Olia, F. Fiori and P. Innocenzi, *Next Mater.*, 2025, **8**, 100756, DOI: 10.1016/j.nxmate.2025.100756.
80 A. Wibrianto, S. Q. Khairunisa, S. C. W. Sakti, Y. L. Ni'mah, B. Purwanto and M. Z. Fahmi, *RSC Adv.*, 2020, **11**(2), 1098–1108, DOI: 10.1039/d0ra09403j.
81 R. M. F. Cardoso, I. M. F. Cardoso, L. Pinto da Silva and J. C. G. Esteves da Silva, *Nanomaterials*, 2022, **12**(7), DOI: 10.3390/nano12071211.
82 Y. Ru, G. I. N. Waterhouse and S. Lu, *Aggregate*, 2022, **3**(6), e296, DOI: 10.1002/agt2.296.
83 Z. X. Liu, Z. L. Wu, M. X. Gao, H. Liu and C. Z. Huang, *Chem. Commun.*, 2016, **52**(10), 2063–2066, DOI: 10.1039/c5cc08635c.
84 R. Guo, Z. Ling, B. Zheng, X. Sun, Z. Yuan and H. Li, *J. Phys. Chem. Lett.*, 2025, **16**(1), 140–147, DOI: 10.1021/acs.jpclett.4c03058.
85 R. Atchudan, T. Edison, K. R. Aseer, S. Perumal, N. Karthik and Y. R. Lee, *Biosens. Bioelectron.*, 2018, **99**, 303–311, DOI: 10.1016/j.bios.2017.07.076.
86 X. Teng, C. Ma, C. Ge, M. Yan, J. Yang, Y. Zhang, P. C. Morais and H. Bi, *J. Mater. Chem. B*, 2014, **2**(29), 4631–4639, DOI: 10.1039/c4tb00368c.
87 B. De and N. Karak, *RSC Adv.*, 2013, **3**(22), 8286–8290, DOI: 10.1039/c3ra00088e.
88 H. S. Tohamy, M. El-Sakhawy and S. Kamel, *Sci. Rep.*, 2023, **13**(1), 11306, DOI: 10.1038/s41598-023-37894-4.
89 K. J. Mintz, M. Bartoli, M. Rovere, Y. Zhou, S. D. Hettiarachchi, S. Paudyal, J. Chen, J. B. Domena, P. Y. Liyanage, R. Sampson, D. Khadka, R. R. Pandey, S. Huang, C. C. Chusuei, A. Tagliaferro and R. M. Leblanc, *Carbon*, 2021, **173**, 433–447, DOI: 10.1016/j.carbon.2020.11.017.
90 A. B. Siddique, A. K. Pramanick, S. Chatterjee and M. Ray, *Sci. Rep.*, 2018, **8**(1), 9770, DOI: 10.1038/s41598-018-28021-9.
91 E. Sturabotti, V. Di Lisio, L. Cardo, A. Camilli, E. Moretón Alfonsín, D. Cangialosi, A. Iturrospe Ibarra, A. Arbe and M. Prato, *Adv. Mater.*, 2025, DOI: 10.1002/adma.202510992.
92 M. B. Prado, N. T. Truong and A. K. Wanekaya, *Sensors Actuators Rep.*, 2023, **6**, 100165, DOI: 10.1016/j.snr.2023.100165.
93 A. Hemmati, H. Emadi and S. R. Nabavi, *ACS Omega*, 2023, **8**(23), 20987–20999, DOI: 10.1021/acsomega.3c01795.
94 C. Sun, Y. Zhang, P. Wang, Y. Yang, Y. Wang, J. Xu, Y. Wang and W. W. Yu, *Nanoscale Res. Lett.*, 2016, **11**(1), 110, DOI: 10.1186/s11671-016-1326-8.
95 Y. Xu, D. Li, M. Liu, F. Niu, J. Liu and E. Wang, *Sci. Rep.*, 2017, **7**(1), 4499, DOI: 10.1038/s41598-017-04754-x.
96 N. A. Travlou, D. A. Giannakoudakis, M. Algarra, A. M. Labella, E. Rodríguez-Castellón and T. J. Bandosz, *Carbon*, 2018, **135**, 104–111, DOI: 10.1016/j.carbon.2018.04.018.
97 T. Teymoorian, N. Hashemi, M. H. Mousazadeh and Z. Entezarian, *SN Appl. Sci.*, 2021, **3**(3), 305, DOI: 10.1007/s42452-021-04287-z.
98 J. F. Moulder, W. F. Stickle, P. E. Sobol and K. D. Bomben, *Handbook of X Ray Photoelectron Spectroscopy: A reference book of standard spectra for identification and interpretation of XPS Data*, Physical Electronics, Eden Prairie, Minn, 1995.
99 A. Bunge, L. Magerusan, I. Morjan, R. Turcu, G. Borodi and J. Liebscher, *J. Nanopart. Res.*, 2015, **17**(9), 379, DOI: 10.1007/s11051-015-3167-2.
100 D. Benchoam, E. Cuevasanta, M. N. Moller and B. Alvarez, *Antioxidants*, 2019, **8**(2), 48, DOI: 10.3390/antiox8020048.
101 W. A. Pryor, *J. Am. Chem. Soc.*, 2002, **82**(18), 4794–4797, DOI: 10.1021/ja01503a010.
102 W. F. Giggenbach, *Inorg. Chem.*, 2002, **13**(7), 1730–1733, DOI: 10.1021/ic50137a039.
103 D. A. Islam, K. Barman, S. Jasimuddin and H. Acharya, *Nanoscale*, 2019, **11**(16), 7560–7566, DOI: 10.1039/c9nr00782b.
104 D. Macabrey, J. Joniova, Q. Gasser, C. Bechelli, A. Longchamp, S. Urfer, M. Lambelet, C. Y. Fu, G. Schwarz, G. Wagnieres, S. Deglise and F. Allagnat, *Front. Cardiovasc. Med.*, 2022, **9**, 965965, DOI: 10.3389/fcvm.2022.965965.
105 X.-L. Wei, Q.-L. Shi, L. Jiang and Y. Qin, *New J. Chem.*, 2023, **47**(33), 15525–15533, DOI: 10.1039/d3nj02694a.
106 Y. Xu, M. Wu, X. Z. Feng, X. B. Yin, X. W. He and Y. K. Zhang, *Chemistry*, 2013, **19**(20), 6282–6288, DOI: 10.1002/chem.201204372.
107 H. Zheng, Q. Wang, Y. Long, H. Zhang, X. Huang and R. Zhu, *Chem. Commun.*, 2011, **47**(38), 10650–10652, DOI: 10.1039/c1cc14741b.
108 Y. Lou, X. Hao, L. Liao, K. Zhang, S. Chen, Z. Li, J. Ou, A. Qin and Z. Li, *Nano Sel.*, 2021, **2**(6), 1117–1145, DOI: 10.1002/nano.202000232.
109 C. Deeney, S. Wang, S. A. Belhout, A. Gowen, B. J. Rodriguez, G. Redmond and S. J. Quinn, *RSC Adv.*, 2018, **8**(23), 12907–12917, DOI: 10.1039/c7ra13383a.